Supplementary Information: Effects of non-halogenated solvent in the main properties of a solution-processed polymeric thin film: a computational study

Karlisson Rodrigo de Almeida Sousa[a],[*] Leandro Benatto[a], Luana Cristina
Wouk de Menezes[ab], Lucimara Stolz Roman[a], and Marlus Koehler[a†]

[a] *Department of Physics, Federal University of Paraná, Curitiba 81531-980, Paraná, Brazil*

[b] *Center of Innovations – CSEM Brazil,*
Belo Horizonte 31035-536, Minas Gerais, Brazil

[*] sousakra@gmail.com

[†] koehler@fisica.ufpr.br

CONTENTS

I. COMPUTATIONAL SIMULATION DETAILS

All force field parameters were adapted from the OPLS table, presented in Tab. S1, and the missing values were obtained by DFT approaches.

A. Solvent simulations

The two different simulations of each solvent, *i.e.* AA and UA model, were done as follows. In a cubic box of dimensions of $(8.0\times8.0\times8.0)$ nm^3 for halogenated solvent and $(10.0\times10.0\times10.0)$ nm^3 for non-halogenated solvent, 1000 molecules were randomly inserted. The MD simulation of each solvent was carried out in the following steps:

  i) *energy minimization* during 1×10^7 steps of iteration using the steepest descent method in the ensemble NVE (without temperature and pressure control) to avoid overlapping of particles and;

  ii) *thermodynamic equilibrium* in the isothermal-isobaric ensemble (NPT) over 20.0 ns with $T = 298.15$ K and $P = 1.0$ atm controlled by Nosé-Hoover[1] thermostat and MTTK[2, 3] barostat, respectively.

The periodic boundary condition (PBC) in all three directions and the treatment of the long-range interactions in the PME method were employed in all solvent simulations.

Table S1. Parameters adapted from the OPLS force field and used in the theoretical model of this study. All values are available inside the GROMACS directory. Partial atomic charges are applied directly from molecular optimizations in DFT/ωB97XD/6-31G(d,p).

Material	OPLS name	type	mass [u]	σ_{ii} [nm]	ε_{ii} [kJ mol^{-1}]
PTB7-Th	opls_1013	C0	12.011	0.355	0.292
	opls_568b	CS	13.019	0.367	0.292
	opls_1010b	C2	14.027	0.390	0.494
	opls_068b	C3	15.035	0.390	0.732
	opls_236	O	15.999	0.296	0.878
	opls_164	F	18.998	0.294	0.255
	opls_633b	S	32.060	0.355	1.046
o-DCB	opls_1013	C0	12.011	0.355	0.292
	opls_1014	C1	13.019	0.367	0.460
	opls_1012	Cl	35.453	0.340	1.255
o-MA	opls_1013	C0	12.011	0.355	0.292
	opls_1014	C1	13.019	0.367	0.460
	opls_068b	C3	15.035	0.390	0.732
	opls_236	O	15.999	0.296	0.878

Newton's equations of motion were iterated using the velocity-Verlet[4] integration method with a time increment of 1.0 fs (2.0 fs) for the AA (UA) model.

B. Simulation of solvent evaporation

In the solvent evaporation process, the PBC was considered only in two directions (X and Y). Temperature and pressure are the same as for solvent validation. So, 100 PTB7-Th oligomers with 12 repeating units were randomly inserted in a box of dimensions (10.0×10.0×60.0) nm^3. Then, this box was filled with previously simulated and equilibrated solvent, where 19931 molecules of o-DCB in the first system (S1) and 17274 molecules of o-MA in the second system (S2) was inserted, resulting in a total of 229048 and 225066 particles in the S1 and S2 systems, respectively. These same boxes were tripled in the Z-axis

with empty boxes above and below for possible solvent flows and avoid contact of the solute with its image in the Z-axis (slab type geometry[5]). Moreover, this technique also preserves the top and bottom surfaces of each film.

II. RESULTS

A. Isolated solvents

Volume: Some time evolution snapshots of the volume of simulation for both solvents described above are shown in Fig. S1.
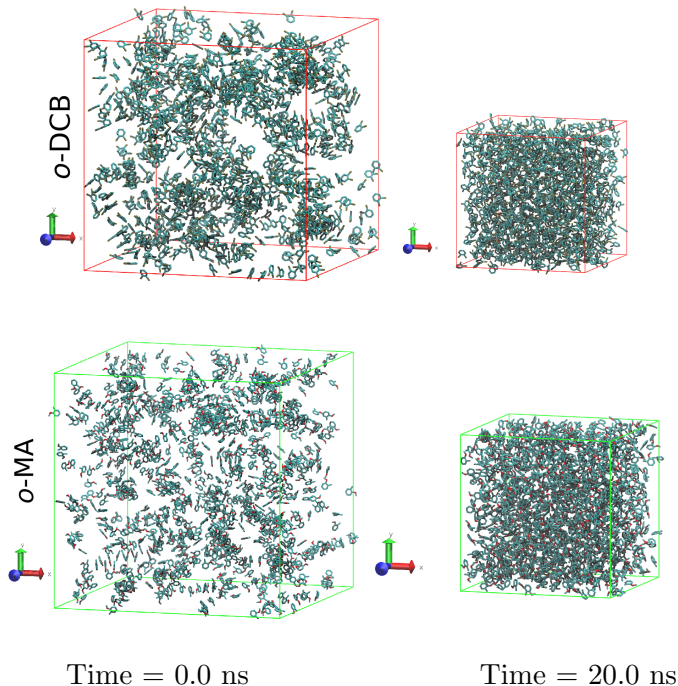

Figure S1. Molecular dynamics snapshots of 1000 molecules of o-DCB (top) and o-MA (bottom) in the NPT ensemble with $P = 1.0$ atm and $T = 298.15$ K, both in the united atoms representation. The figures on the left are the initial structures ($t = 0.0$ ns) and figures on the right of final structures ($t = 20.0$ ns).

Energies and densities: Figs. S2 (a) and (b) show the time evolution of the total energy per particle and density of mass for both solvents. From the total energy, we see that thermodynamic equilibrium was reached even in the first nanosecond of MD. Consequently, there is no more variation in its volume, as can be seen in the mass density (Fig. S2 (b)).
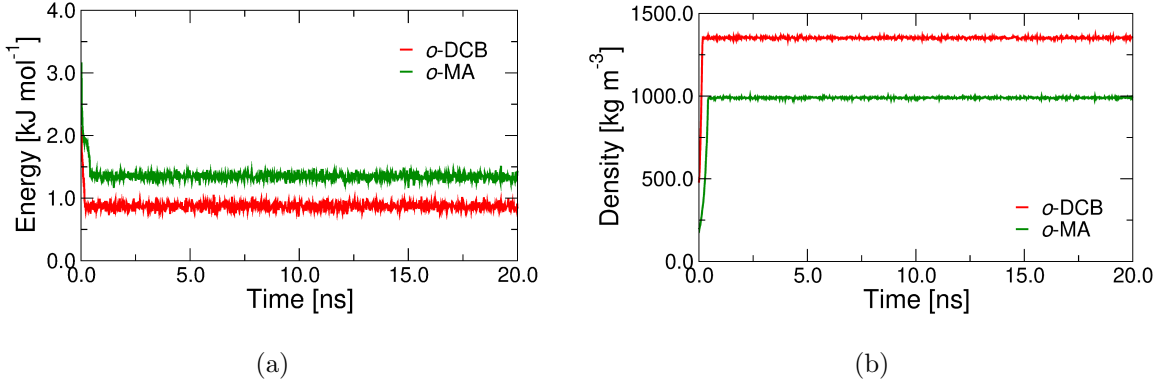
4

Figure S2. Time-dependent evolution of (a) total energy (per particle) and (b) density of mass during the molecular dynamics simulation of o-DCB and o-MA solvents.

The variation of vaporization enthalpy (cited in the main text) is given by

$$\Delta H_{\mathrm{vap}} = H_{\mathrm{gas}} - H_{\mathrm{liquid}} \tag{1}$$

where $H = E_{\mathrm{total}} + pV$ in the liquid and gaseous state. However, for an ideal gas $pV = RT$. Applying these considerations the Eq. (1) becomes

$$\Delta H_{\mathrm{vap}} = [E_{\mathrm{total}} + RT]_{\mathrm{gas}} - H_{\mathrm{liquid}} \;, \tag{2}$$

where R is the gas constant and T is the temperature.

B.   Simulated solvent evaporation

Energy from non-bonded interactions: The time evolution of energies from the non-bonded interactions during the MD is shown separately in Fig. S3. Both LJ and electrostatic energies converged to a close value in these systems. Therefore, there is no significant difference between them.

Energy from bonded interactions: The angle and dihedral energies (see Figs. S4 (b) and (c)) contribute to the total energy difference with small values; $\Delta E_{\mathrm{angle}} \approx 5.9 \times 10^2$ kJ mol^{-1} and $\Delta E_{\mathrm{dihedral}} \approx 9.96 \times 10^2$ kJ mol^{-1}, respectively. Finally, we have the bond energies, Fig. S4 (a). In the first nanosecond of simulation, the energy difference between the two systems is high but quickly decreases to an almost constant value around $\Delta E_{\mathrm{bond}} \approx 1.6 \times 10^4$ kJ mol^{-1} (the largest contribution to the energy difference). What happens in this first moment is a classical geometry optimization.
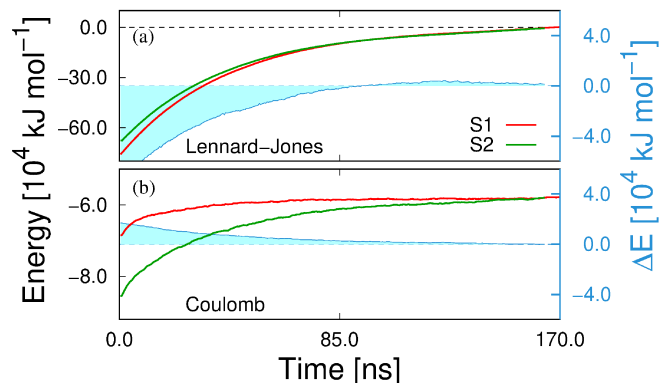
Figure S3. Time evolution of potential energy (a) from the van der Waals forces, described in this model by Lennard-Jones equation, and (b) from the electrostatic interactions. The values refer to all particles in the system at a given time. The energy difference, *i.e.* $E(\text{S1})$ - $E(\text{S2})$, is represented by the blue curve.

Energy from polymer-solvent interactions: Van der Waals (LJ) and electrostatic interactions are higher for the S1 system because it has a higher density of mass compared to S2. The fact that LJ energy is more negative in Fig. S5 indicates that the system components are more attractive to each other. In this case, the halogenated solvent o-DCB has a stronger interaction with PTB7-Th than the green solvent.

Energy from bond lengths: In principle, to study all covalent bonds of oligomers
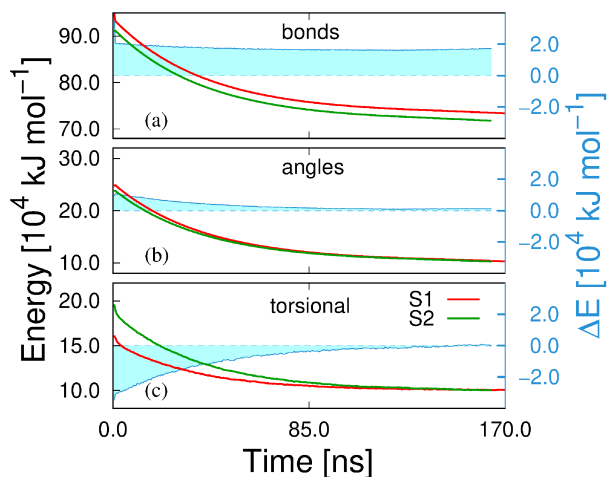

Figure S4. Time-dependent evolution of bonded interaction energies among all particles in the systems S1 (with halogenated solvent) and S2 (with non-halogenated solvent) at a given time. The torsional energy refers to the proper and improper dihedral.
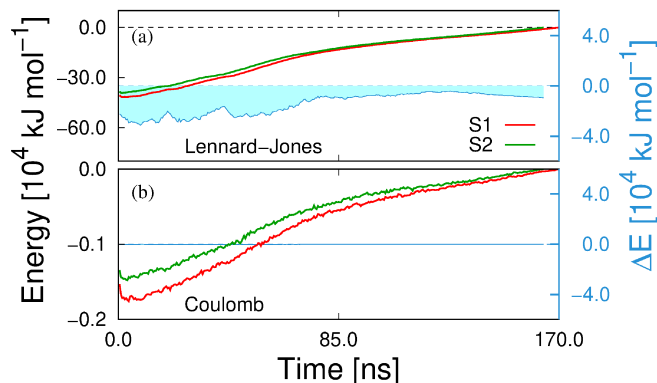
6

Figure S5. Time evolution of potential energy (a) from the van der Waals forces and (b) from the electrostatic interactions. The interaction occurs between the solvent and the solute.

involves verifying more than 77×10^3 bonds. Therefore, we checked only the bonds involving atoms that have the greatest number of degrees of freedom for a possible variation of the initial parametrization. For example, the identification (or index) of each pair of atoms mainly involved in thiophene bonds were isolated (see Fig. S6 (a)), resulting in 5 files to be used in GROMACS. Since the oligomer contains 12 repetition units, 12 bonds of each listed type[‡], out of 100 oligomers, result in 1200 identifications of atom pairs in each of these 5 files. Then, another script containing commands to be used in GROMACS was used to measure the bonding length for each pair of atoms listed in the 5 files. This results in 5900 new files. The average bonding length in each file is calculated using another script in GNUPLOT and following plotting the graph in Fig. S6 (b). Therefore, each point on this graph is an average of the bonding length of the same pair of atoms in a PTB7-Th oligomer during the last 0.5 ns of MD. The line among the points is the value initially set during parametrization/optimization with DFT. The same process is valid in Figs. S6 (c) and (d) for other analyzed bonds.

C.   Thin film morphology

Density of mass: We measured the density of mass of each thin film resulting from solvent evaporation through some analysis. One of them is related to the thickness of the polymeric thin film. For that, we obtained the density of mass along the Z-axis, shown

---

[‡] Except for the CT5-CT1 bond, as this is the bridge between two units, so there are only 11 such bonds in each oligomer.
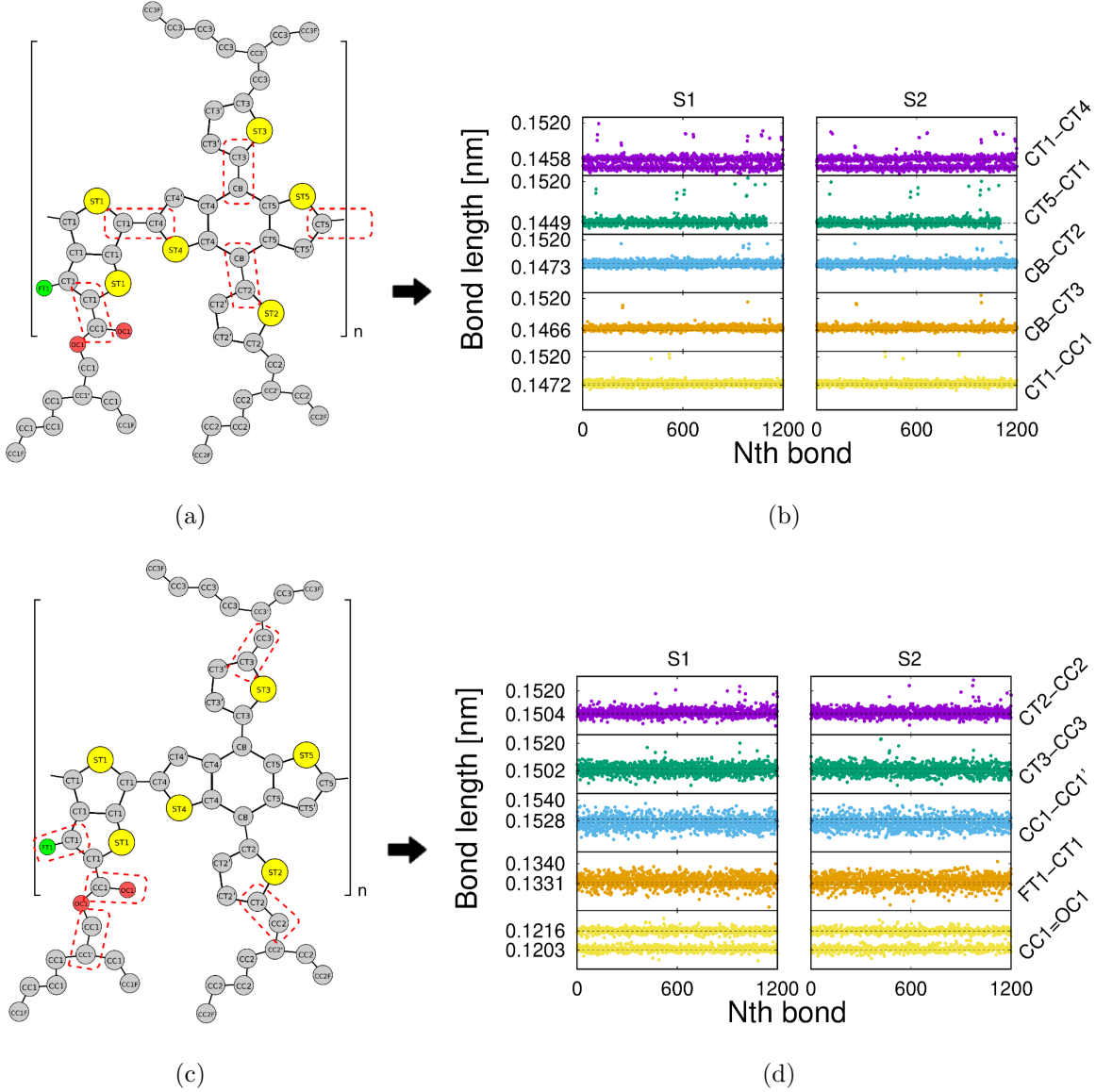
7

(a)

(b)

(c)

(d)

Figure S6. Representative scheme of some selected covalent bonding lengths ((a) and (c)) and their computed lengths ((b) and (d)). At the right-hand graphs, each point represents the average time, of the last 0.5 ns of MD, of each covalent bond of the 100 PTB7-Th oligomers. The dashed lines represent the initial bond length values defined during the material parametrization.

in Fig. S8 (a). It was found that the system S1 has a thickness of 17.482 nm and the system S2, 17.964 nm. As can be seen in Fig. S8 (b), the polymeric chains are more stretched in the system S2, where we present the average distance between the ends of each oligomer, justifying the difference in the previous result. The solvent-accessible surface area (SASA), Fig. S8 (c), of the second system also showed slightly higher values. These three results indicate a lower mass density of the thin film processed with non-halogenated solvent (S2).
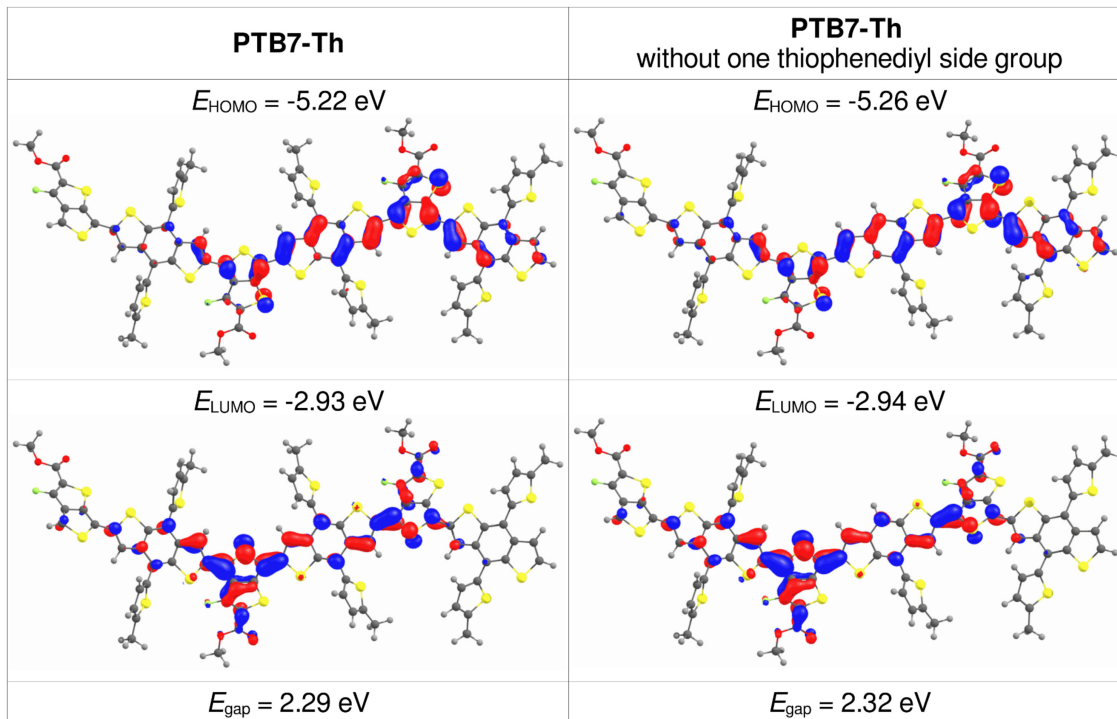
Figure S7. Frontier molecular orbitals and the respective energies of PTB7-Th with three repetition units calculated with M06[6] functional and 6-31G(d,p) basis set following previous works[7, 8] (the energy levels are in agreement with experimental results of ref.[9] obtained from electrochemical cyclic voltammetry, E_{HOMO} = -5.36 eV, E_{LUMO} = -3.43 eV, and E_{gap} = 1.93 eV).

Radial distribution of pairs: We calculated the centers of mass (CM) of some PTB7-Th atom groups using a Fortran routine to analyze the pair correlation function ($g(r)$) in the simulated systems, see Fig. S9 (a). To avoid short distance noise in the $g(r)$ due to CMs in the same oligomer, it was necessary to consider only CM pairs of different oligomers. Although the resulting films already have solid aspects, the distribution in the first solvation layer shown in Fig. S9 (b) is below 1.0. This is because the CMs are not considered along the one oligomer backbone and the pair correlation function has a spherical rather than cylindrical normalization. It is okay to consider spherical normalization and the only difference is the peak height.
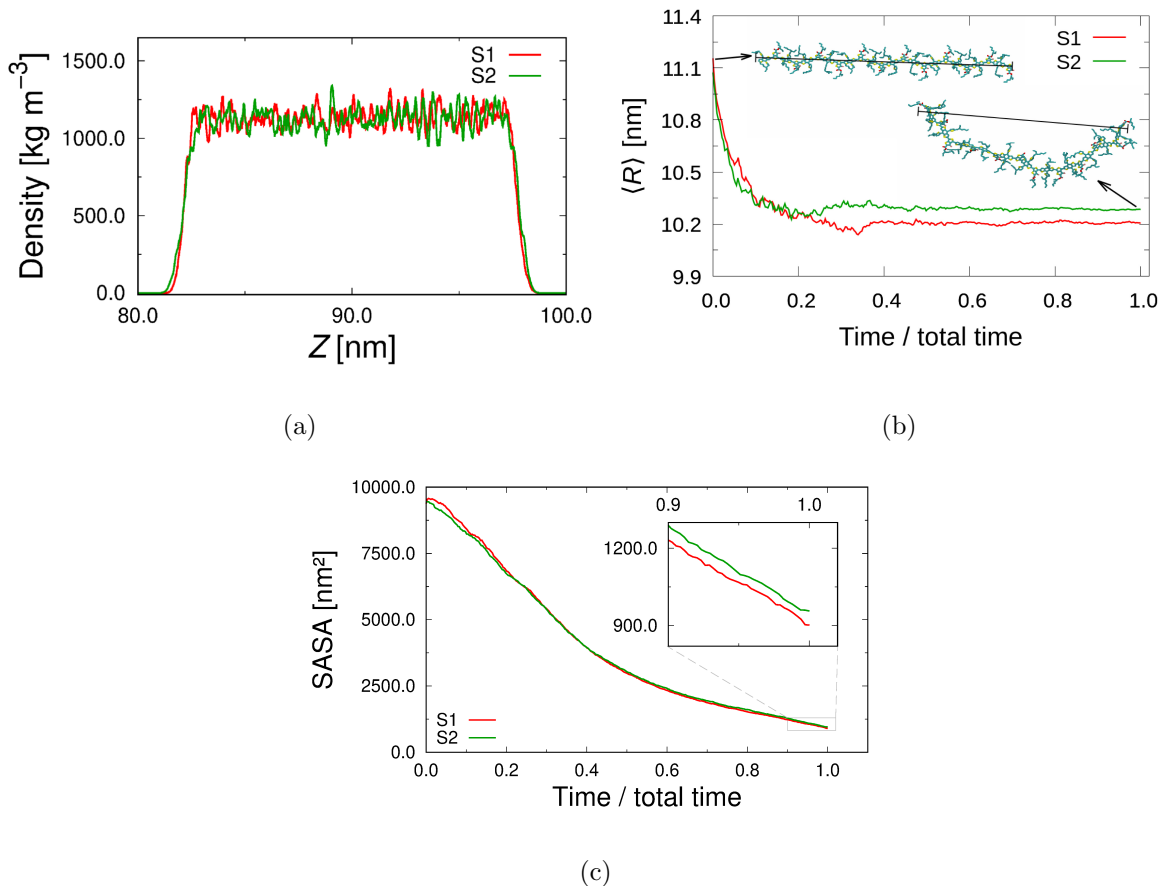
9

(a)   (b)

(c)

Figure S8. Analysis for the film thickness: (a) density of mass through the Z-axis for both systems. Values from 0.0 to 80.0 and from 100.0 to 180.0 nm are null and were omitted. (b) Normalized time evolution of the end-to-end distance of the PTB7-Th oligomers in both solvents. Each point is an average of end-to-end distance of 100 oligomers over 0.5 ns of MD. (c) Normalized time evolution of solvent-accessible surface area around the oligomers.

D. Hole mobility of the thin film

Calculation of the reorganization energy: The intramolecular component of reorganization energies[8] λ_h (for holes) can be evaluated by:

$$\lambda_h = (E_0^+ - E_+^+) + (E_+^0 - E_0^0) , \tag{3}$$

where E_0^+ and E_+^+ is the energy of the cation calculated with the optimized structure of the neutral molecule and the energy of the cation calculated with the optimized cation structure; E_+^0 and E_0^0 is the energy of the neutral molecule calculated in the cationic state and the energy of the neutral molecule at the ground state structure. These calculations
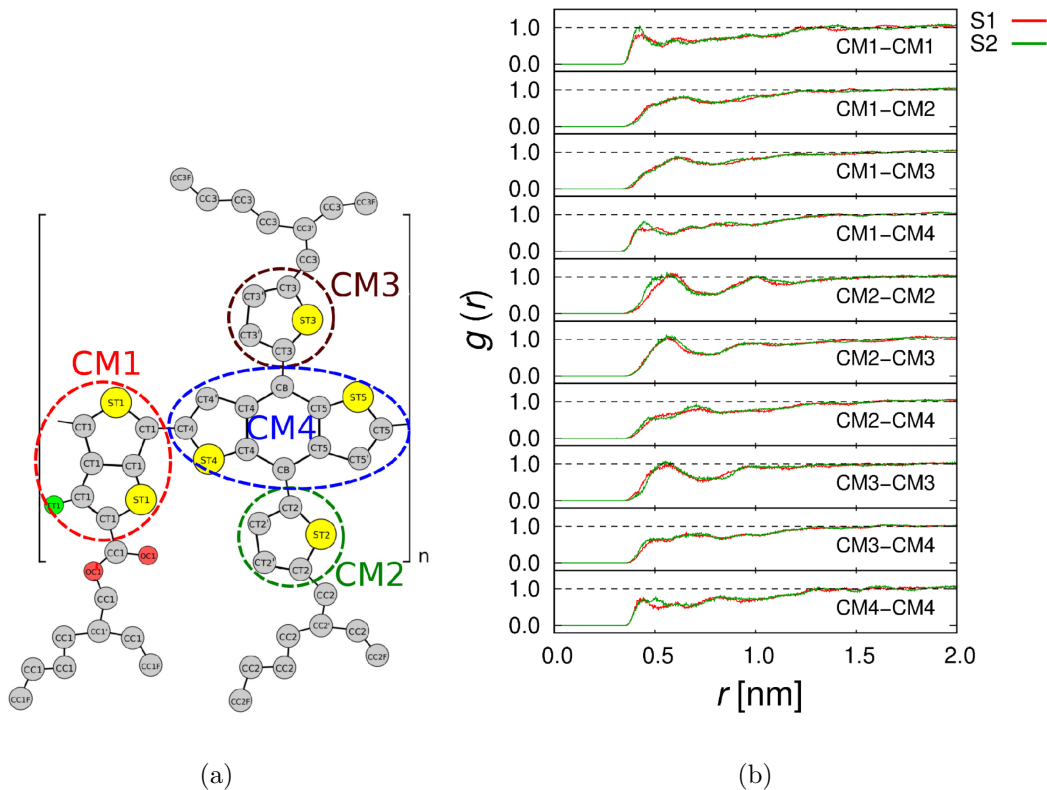
10

Figure S9. (a) Representation of the centers of mass (CM) of some parts of PTB7-Th oligomers and (b) their pair correlation function.

were done with the B3LYP[10] functional and 6-31G(d,p) basis set,[11] in agreement with other works.[7, 12, 13]

Calculation of the transfer integral: The procedure to obtain the electronic coupling between each dimer was as follows. First, a geometry optimization was performed via DFT/ωB97XD/6-31G(d,p) of a PTB7-Th dimer containing 3 repetition units each. After we obtained the t_h magnitude for this dimer from a fragment orbital analysis,[14] from the electronic coupling between the highest occupied molecular orbitals (HOMOs).[8] Then we increase the distance between the two oligomers and calculate the magnitude of t_h for two more positions. From these results, it was possible to obtain the behavior of t_h as a function of the interaction distance between the oligomers. The result presented in Fig. S10 was an exponential decrease, $e^{(-\alpha x)}$, where $\alpha = 2.1$ Å^{-1}. This is a characteristic behavior of organic systems. From the parametrization of t_h as a function of the interaction distance between the oligomers, it will be possible to associate a value of t_h for each value of R_{inter}. This procedure was designed to significantly reduce the high computational cost that involves

the individual calculation of t_h for each pair of oligomers considered in the MD. Remember that 100 oligomers were considered, resulting in a total of 4950 pair combinations.

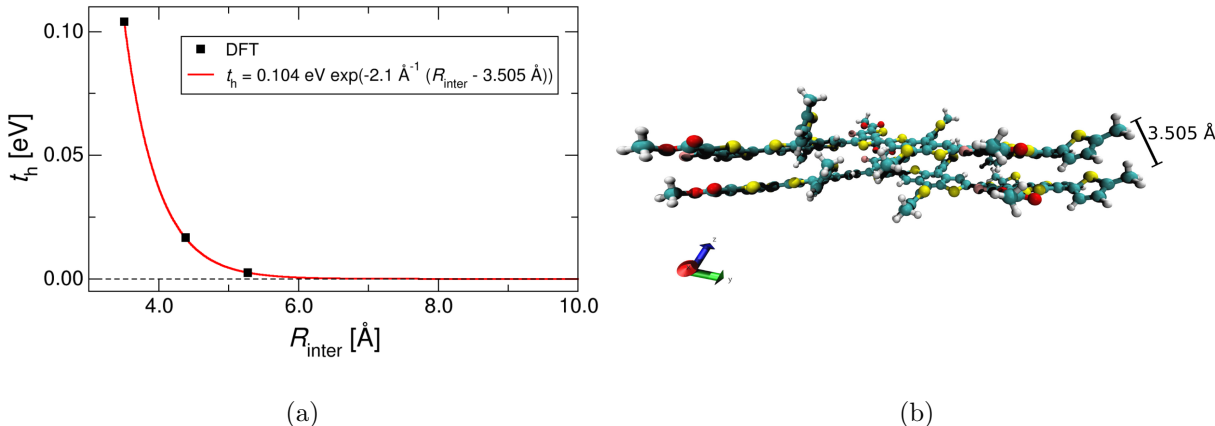(a)   (b)

Figure S10. (a) Electronic coupling intensity as a function of the interaction distance between two oligomers. The squares are the DFT results from fragment orbital analysis and the red line is the exponential curve fitting, $e^{(-\alpha R)}$, using the initial energy value of the first point at distance 3.505 Å. The best fit was achieved with $\alpha = 2.1$ Å^{-1}. (b) Snapshot of two oligomers separated by 3.505 Å.

Calculation of the distance between oligomers: The distances R_{inter} among CMs (see Fig. S9 (a)) were calculated only for different oligomers to avoid "hop" counting along the same backbone. Then, only the shortest distance (and the coordinates of the respective CMs involved) between two oligomers is stored for later use in Monte Carlo simulation. Since HOMO orbitals, responsible for hole mobilities, are present on the backbone (see Fig. S7), were considered only the centers of mass CM1 and CM4 in the MC simulations.

Monte Carlo simulation protocol: Mean Squared Displacement (MSD) was calculated by obtaining the random hole percolation path through the polymer CMs. This path was redone from the random origin point (R_0) $N_{\text{repetitions}} = 1 \times 10^4$ times and its MSD stored in an output file. Each percolation path occurred through $N_{\text{jumps}} = 1 \times 10^5$ jumps and the possibilities of each hop was the first 20 nearest neighboring CMs. Summarizing, we have the following average

$$\langle [R(t) - R(0)]^2 \rangle \equiv \frac{1}{N_{\text{repetitions}}} \sum_{j=1}^{N_{\text{repetitions}}} \left\{ \sum_{i=1}^{N_{\text{jumps}}} [R_i(t) - R_j(0)]^2 \right\}_j . \tag{4}$$

The choice between the 20 neighbors and the probability test (see the main text) was performed using random numbers from a uniform distribution of values from 0 to 1.0, as we can see in Fig. S11 for 1×10^6 repetitions.
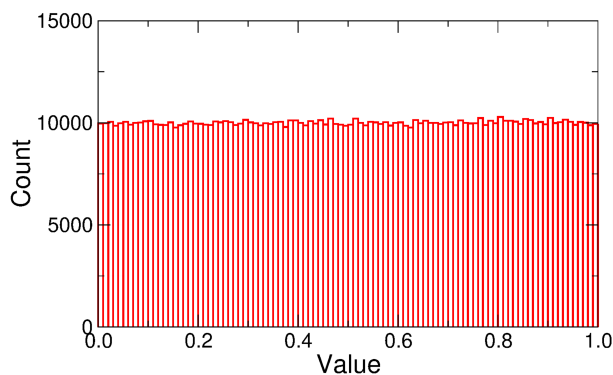
Figure S11. Uniform distribution of random numbers from the Fortran random_number routine. In this case, the routine has been called 1×10^6 times.

---

[1] W. G. Hoover, *Physical review A*, 1985, **31**, 1695.

[2] G. J. Martyna, M. E. Tuckerman, D. J. Tobias and M. L. Klein, *Molecular Physics*, 1996, **87**, 1117–1157.

[3] M. E. Tuckerman, J. Alejandre, R. López-Rendón, A. L. Jochim and G. J. Martyna, *Journal of Physics A: Mathematical and General*, 2006, **39**, 5629.

[4] W. C. Swope, H. C. Andersen, P. H. Berens and K. R. Wilson, *The Journal of Chemical Physics*, 1982, **76**, 637–649.

[5] B. S. Daan Frenkel, *Understanding Molecular Simulation: From Algorithms to Applications*, Academic press, San Diego, 2nd edn, 2002, p. 638.

[6] Y. Zhao and D. G. Truhlar, *Theoretical Chemistry Accounts*, 2008, **120**, 215–241.

[7] L. Benatto, C. F. Marchiori, C. M. Araujo and M. Koehler, *Journal of Materials Chemistry C*, 2019, **7**, 12180–12193.

[8] L. Benatto and M. Koehler, *The Journal of Physical Chemistry C*, 2019, **123**, 6395–6406.

[9] Y. Lin, F. Zhao, Q. He, L. Huo, Y. Wu, T. C. Parker, W. Ma, Y. Sun, C. Wang, D. Zhu *et al.*, *Journal of the American Chemical Society*, 2016, **138**, 4955–4961.

[10] A. D. Becke, *The Journal of Chemical Physics*, 1993, **98**, 5648–5652.

[11] V. Coropceanu, M. Malagoli, D. da Silva Filho, N. Gruhn, T. Bill and J. Brédas, *Physical review letters*, 2002, **89**, 275503.

[12] G. Han, Y. Guo, X. Song, Y. Wang and Y. Yi, *Journal of Materials Chemistry C*, 2017, **5**,

4852–4857.

[13] J. Idé, D. Fazzi, M. Casalegno, S. V. Meille and G. Raos, *Journal of Materials Chemistry C*, 2014, **2**, 7313–7325.

[14] H. Oberhofer, K. Reuter and J. Blumberger, *Chemical reviews*, 2017, **117**, 10319–10357.